Thermodynamics of small clusters of atoms: A molecular dynamics simulation

Damgaard Kristensen, W.; Jensen, E. J.; Cotterill, Rodney M J

Published in:
Journal of Chemical Physics

Link to article, DOI:
10.1063/1.1680883

Publication date:
1974

Document Version
Publisher's PDF, also known as Version of record

Thermodynamics of small clusters of atoms: A molecular dynamics simulation

W. Damgaard Kristensen, E. J. Jensen, and R. M. J. Cotterill

Department of Structural Properties of Materials, The Technical University of Denmark, Building 307, DK-2800 Lyngby, Denmark

(Received 31 October 1973)

The thermodynamic properties of clusters containing 55, 135, and 429 atoms have been calculated using the molecular dynamics method. Structural and vibrational properties of the clusters were examined at different temperatures in both the solid and the liquid phase. The nature of the melting transition was investigated, and a number of properties, such as melting temperature, latent heat of melting, and premelting phenomena, were found to vary with cluster size. These properties were also found to depend on the structure of the solid phase. In this phase the configuration of lowest free energy was found to be icosahedral in the 55-atom system and face centered cubic for the two larger systems.

I. INTRODUCTION

The thermodynamic properties of very small clusters of atoms are of great importance for the understanding of a number of physical problems, including those of nucleation and crystal growth. Calculations of the stability and structure of such microcrystals have usually been based on static models, and the zero-temperature properties thus derived have been extrapolated to finite temperatures within the framework of the harmonic approximation. Recently dynamical calculations of the Monte Carlo and molecular dynamics type applied to small atom clusters have been reported. Using these methods the anharmonic behavior at higher temperatures can be treated exactly.

Allpress and Sanders[1] calculated the minimum energy of different structures containing up to about 2000 atoms by uniformly scaling the microcrystal. The method was refined by Burton[2,3] allowing for more realistic relaxations of the atoms. The resulting configurations were used to calculate the heat capacity, energy, and entropy. Abraham and Dave[4,5] were able to develop a modified Einstein model giving results which were in agreement with those of Burton. Recently Hoare and Pal[6] have presented the results of a study involving completely free relaxation of all atoms in assemblies of between 4 and 70 atoms. They calculated the thermodynamic properties of these clusters using the harmonic approximation. The inherent limitations of the harmonic approximation, such as its restriction to a single configuration[7] and the neglect of anharmonic effects, can be overcome by a dynamical treatment.

Dickey and Paskin[8] have used the molecular dynamics technique to calculate the low temperature phonon properties of systems having different surface to volume ratios and this allowed them to identify the characteristic surface modes. Cotterill *et al.*[9] used the same method to calculate the thermodynamic properties of two-dimensional microclusters (microcrystals and microdroplets) at higher temperatures, and they investigated the nature of the melting transition. A similar procedure was adopted by Briant and Burton[10] in their study of the melting transition of the three-dimensional 55-atom cluster. McGinty,[11] using the molecular dynamics technique, and Lee *et al.*,[12] using the Monte Carlo method, have calculated free energies of formation of clusters of up to 100 atoms for a number of different temperatures.

The object of the work described in the present paper was to derive the thermodynamic properties of three-dimensional microclusters at higher temperatures, with special emphasis being given to the characteristics of the melting transition. Although the interatomic interactions were represented by the Lennard-Jones pair potential, appropriate to a certain extent to the noble gases (to which comparison is made), the gross features exhibited by this model are believed to be of a more fundamental nature and are probably not significantly affected by the finer details of the interatomic interaction.

II. MODEL AND COMPUTATIONAL PROCEDURE

Three different cluster sizes were considered, containing 55, 135, and 429 atoms. The atoms were initially arranged in the face-centered cubic structure by adding 4, 7, and 16 closed neighbor shells respectively around a central atom. The interaction between the individual atoms was calculated using the Lennard-Jones potential

$$V(r) = \epsilon[(r_0/r)^{12} - 2(r_0/r)^6] \tag{1}$$

truncated midway between the fourth and fifth neighbor shell distance, i.e.,

$$V(r) = 0 \text{ for } r > r_{\text{trc}} ,$$
$$r_{\text{trc}} = (4.5)^{1/2} r_0 . \tag{2}$$

The dynamical simulation of the equilibrium thermodynamical properties of the atom clusters was carried out by means of the molecular dynamics technique[13–15] in which the set of coupled differential equations governing the classical atomic motions were solved. A central difference approximation was used in the present calculations

$$\bar{r}_i(t+\Delta t) = 2\bar{r}_i(t) - \bar{r}_i(t-\Delta t) + \bar{a}_i(t)\Delta t^2 \tag{3}$$

giving the position of the ith atom at the time $t+\Delta t$ from knowledge of the instantaneous position $\bar{r}_i(t)$ and acceleration $\bar{a}_i(t)$ and of the position $\bar{r}_i(t-\Delta t)$ of this atom one time step Δt earlier. The acceleration is readily obtained

as the sum of contributions arising from those atoms situated inside the truncation sphere of the ith atom.

Reduced variables, according to the convention

$$\epsilon = r_0 = M = k_B = 1 ,$$

were used throughout and the results will be presented in these units. ϵ and r_0 are the parameters of the Lennard-Jones potential, M the atomic mass, and k_B Boltzmann's constant.

Introduction of these units yields the following expressions for various statistical mechanical relations:

$$E_{\text{pot}} = \frac{1}{2N} \sum_i \sum_j (r_{ij}^{-12} - 2r_{ij}^{-6}) - \varphi_0 , \tag{4}$$

$$E_{\text{kin}} = \frac{1}{2N} \sum_i v_i^2 , \tag{5}$$

for the kinetic and potential energy per atom, where N is the number of atoms in the system, r_{ij} is the distance between the ith and jth atoms, and v_i is the scalar velocity of atom i. φ_0 is chosen so as to give zero potential energy for the relaxed microcrystal (having face-centered cubic structure) at zero temperature. The temperature is defined by

$$T = [3N/(3N-6)]\tfrac{2}{3}E_{\text{kin}} \tag{6}$$

and from the virial theorem the pressure is derived as

$$P = \rho T + \frac{2\rho}{N} \sum_i \sum_j (r_{ij}^{-12} - r_{ij}^{-6}) , \tag{7}$$

where ρ is the number density. Throughout, the summation over index i is carried out for all N atoms, while the j summation is performed only for those atoms situated inside the truncation sphere of the ith atom, with the constraint $j \neq i$.

The average nearest-neighbor distance was computed, using a definition of nearest neighbors of a specified atom as those closer to it than $(1.5)^{1/2}$.

The entropy of the system was calculated in two different ways, one of thermodynamic origin, the other being based on a vibrational analysis of the system. From the caloric equation of state, relating the total energy E to the temperature T, the specific heat follows as

$$c_P = \frac{1}{N}\left(\frac{\delta E}{\delta T}\right)_P \tag{8}$$

yielding the entropy difference

$$s(T_2) - s(T_1) = \int_{T_1}^{T_2} \frac{c_P}{T}\, dT . \tag{9}$$

TABLE I. Conversion factors for the Lennard-Jones potential with a 54-neighbor truncation fitted to the noble gas solids using the experimental data[19] for the sublimation energy and lattice parameter at zero temperature. The factors for energy, length, mass, temperature, and time are listed.

	$\epsilon = E^*$ [10^{-14} erg]	$r_0 = r^*$ [10^{-8} cm]	$M = M^*$ [10^{-22} g]	$\epsilon/k_B = T^*$ [10^2 °K]	$\sqrt{r_0^2 M/\epsilon} = t^*$ [10^{-12} sec]
Ar	1.63	3.839	0.66	1.18	2.44
Kr	2.35	4.079	1.39	1.70	3.14
Xe	3.37	4.431	2.18	2.44	3.56

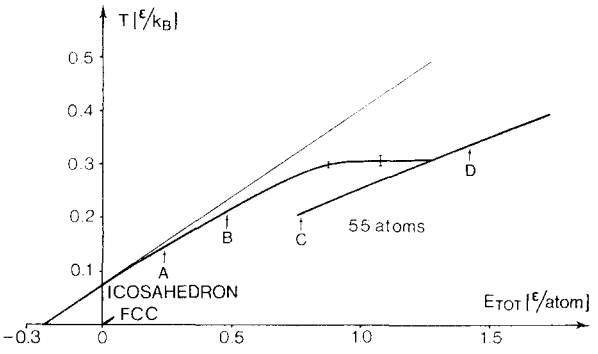

FIG. 1. Caloric equation of state for the 55-atom system. The curve is drawn on the basis of 107 pairs of (E_{TOT}, T) values uniformly distributed along the energy axis. The light line represents equipartition between kinetic and potential energy in the icosahedral system which exhibits a zero temperature energy of -0.2265. The origo is fixed by the zero temperature energy of the isomeric fcc system. The branch ABD represents a heating sequence and includes a flat melting transition region. The branch C is obtained by cooling and represents supercooled liquid states. The low-temperature properties of the metastable fcc system are shown in the branch originating from zero total energy. The uncertainty in temperature is less than ± 0.002, except for the transition region, where an uncertainty of ± 0.010 is observed.

The vibrational analysis leading to an expression for the entropy is based on the result of Dickey and Paskin[16] that the frequency spectrum can be obtained as the Fourier transform of the velocity autocorrelation function

$$\gamma(t) = \left\langle \sum_i \bar{v}_i(t)\bar{v}_i(o) \Big/ \sum_i v_i(o)^2 \right\rangle , \tag{10}$$

where $\bar{v}_i(t)$ is the velocity of the ith atom at time t. The angular brackets imply ensemble averaging.

In a paper concerning different methods of obtaining the entropy of atomic model systems Esbjørn *et al.*[17] use the expression

$$s(T) = \frac{k_B}{N} \int_0^\infty D(\omega) \left(1 + \ln\left(\frac{k_B T}{\hbar\omega}\right)\right) d\omega \tag{11}$$

valid in the classical limit of $k_B T > \hbar\omega$, where

$$D(\omega) = \int_0^\infty \gamma(t) \cos(\omega t)\, dt , \tag{12}$$

which was applied in the present calculations with the normalization condition

$$\int_0^\infty D(\omega)\, d\omega = 3N - 6 \tag{13}$$

corresponding to the $3N-6$ vibrational modes of the cluster of atoms.

The structural properties of the clusters were examined by calculating the pair distribution function[14,18]

$$g(r) = \langle n_i / 4\pi r_i^2 \Delta r_i \rho \rangle , \tag{14}$$

where n_i is the number of atoms in the element Δr_i at a distance r_i, in this case measured from the central atom of the cluster, and ρ is the number density.

The equilibrium thermodynamic properties of each of the three clusters considered were obtained by the following procedure. The atoms of the relaxed face-centered cubic microcrystal were initially given small ran-

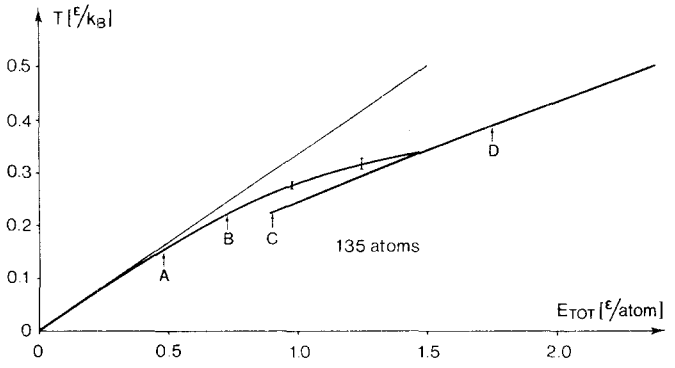

FIG. 2. Caloric equation of state for the 135-atom system. The curve is drawn on the basis of 94 pairs of (E_{TOT}, T) values uniformly distributed along the energy axis. The light line represents equipartition of energy in the fcc system. The curve shows a heating sequence *ABD* which includes a broad transition region together with a cooling branch *C* representing supercooled liquid states. The uncertainty in temperature is less than ± 0.002, except for the transition region, where an uncertainty of ± 0.010 is observed.

dom displacements, and the temporal evolution of the system was calculated by means of the molecular dynamics technique. Every hundredth time step the instantaneous positions and velocities of all the atoms were stored, and subsequently a certain amount of heat was added to the system by increasing the atomic velocities, thus creating a series of data sets representing different values of the total energy of the system. Each data set was then used as the initial condition for a molecular dynamics simulation covering 4000 time steps. Throughout this procedure the time step was chosen to be 0.003 in reduced units (see Table I). Equilibrium thermodynamic properties were extracted from these simulations, and the behavior of the microcrystals for different values of the total energy, covering a range from zero to well above the melting transition, was recorded. In order to ensure good statistics a new data set was stored at the end of the 4000 time step simulation, allowing one to continue the simulation of the microcrystal for another 4000 time steps at that particular value of the total energy. During these 4000 time steps the temperature, pressure, potential energy, and the average nearest-neighbor distance were monitored and at the end of the simulation period mean values of these variables were computed. The entropy was calculated on the basis of the average of eight velocity autocorrelation functions each of which was evaluated over a time interval corresponding to 500 time steps. The onset of evaporation of the cluster was monitored by periodically counting the atoms situated inside a sphere of radius

$$R = R_{\text{syst}} + r_{\text{trc}} , \tag{15}$$

where R_{syst} is the radius of the perfect system.

In order to facilitate comparison with experimental data the conversion factors X^* from dimensionless variables X to cgs units X' are listed in Table I ($X' = X^* X$). The conversion factors are expressed in terms of ϵ, the minimum value of the interatomic potential, and r_0, the separation distance at which the minimum is situated. The appropriate conversion factors for the truncated Lennard-Jones potential, fitted to the noble gases, are given.

III. RESULTS

A variety of physical properties are known to change abruptly upon melting of the bulk material and can thus be used in equilibrium simulations of the present kind to locate the melting transition. As was shown by simulation of two-dimensional microcrystals,[9] the existence of the free surface has the effect of obscuring the changes to such an extent that most of these properties no longer constitute a reliable basis for distinguishing between the solid and liquid phases. It was found, however, that the caloric equation of state can still be used to describe some of the thermodynamic details of the phase transition. This equation of state, which gives the total energy as a function of temperature, was also used in the present analysis of three-dimensional systems and the results of the calculations are shown in Figs. 1–3 for the 55, 135, and 429 atom clusters, respectively. Within a certain range of total energy this function is double-valued. The upper branch is the heating curve and the lower is the cooling curve. The straight lines on these plots represent equipartition between kinetic and potential energy.

It is seen that the 55-atom cluster behaves in a fashion markedly different from that observed in the other two systems, in that the equation of state curve does not originate from the origin that represents the relaxed fcc structure. This difference in behavior reflects the fact that the face-centered cubic structure of the 55-atom cluster is not the structure of lowest energy.[6,20] When heating this structure to a temperature of about 0.05, the system was found to undergo a structural phase transition producing ultimately an icosahedral configuration. The zero temperature potential energy per atom of this configuration was found to be 0.23 less than that of the face-centered cubic configuration. The final caloric equation of state depicted in Fig. 1 was calculated by starting out not from the face-centered cubic

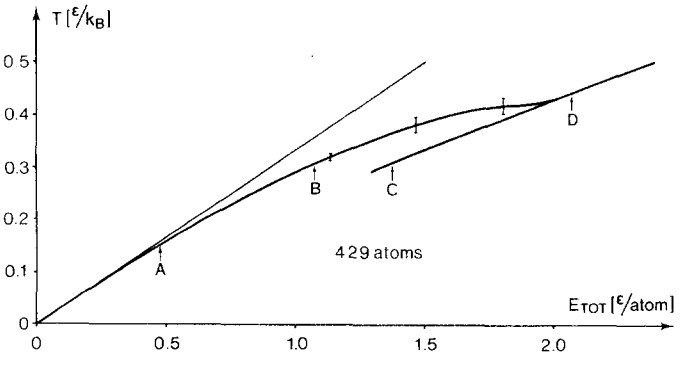

FIG. 3. Caloric equation of state for the 429-atom system. The curve is drawn on the basis of 71 pairs of (E_{TOT}, T) values uniformly distributed along the energy axis. The light line represents equipartition of energy in the fcc system. The curve shows a heating sequence *ABD* which includes a broad transition region together with a cooling branch *C* representing supercooled liquid states. The uncertainty in temperature is less than ± 0.002, except for the transition region, where an uncertainty of ± 0.015 is observed.

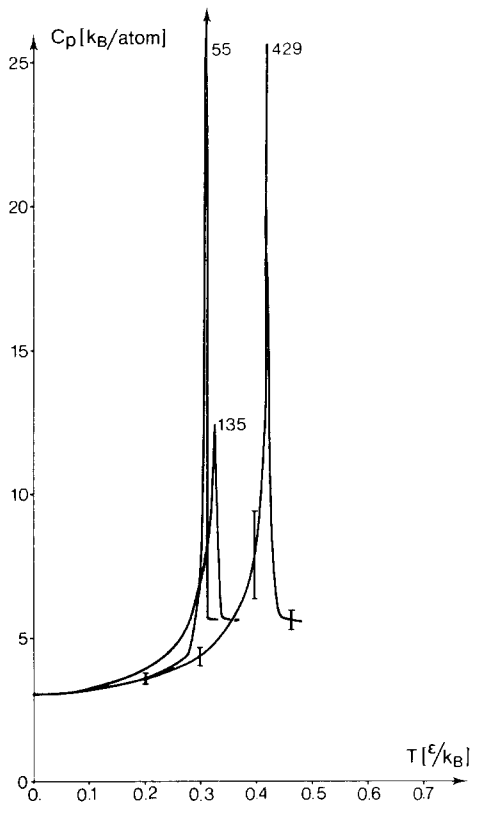

FIG. 4. Specific heat at constant pressure as a function of temperature for the three different cluster sizes. The estimated error is indicated for the larger system only but exhibits the same trend for the smaller systems in that it is roughly determined by the actual C_p value. The maxima exhibit the largest uncertainties which amount to $\sim \pm 10$ for the 4290atom system, $\sim \pm 3$ for the 135-atom system, and for the 55-atom system it can be said only that the maximum value is larger than 25.

structure but from a relaxed icosahedral microcrystal in accordance with the procedure described in Sec. II.

In Fig. 4 the specific heat at constant pressure, derived from the caloric equation of state using Eq. (8), is shown for the three systems. These curves give directly the positions of the melting transitions of the different clusters and show that the melting temperature is an increasing function of the size of the cluster. A state resembling premelting is observed and is found to be less pronounced for the icosahedral systems than for the face-centered cubic systems. If the melting temperature T_M is defined as the temperature at which the specific heat attains its maximum value, the resulting T_M for the 55, 135, and 429 atom systems are 0.310, 0.325, and 0.420, respectively.

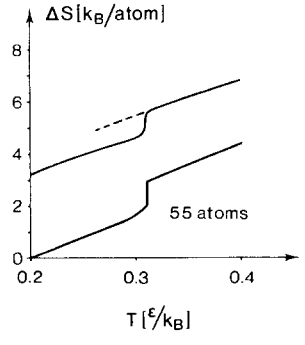

FIG. 5. Entropy variation with temperature for the 55-atom system. The upper curve is derived from vibrational spectra corresponding to the calculated points of the caloric equation of state. The uncertainty in entropy is ± 0.1. The lower curve is derived by integration of the specific heat curve. The accumulated error is estimated to reach a value of ± 0.2 at the highest temperature, whereas the accuracy of the entropy of fusion which is given by a local entropy difference is about ± 0.02.

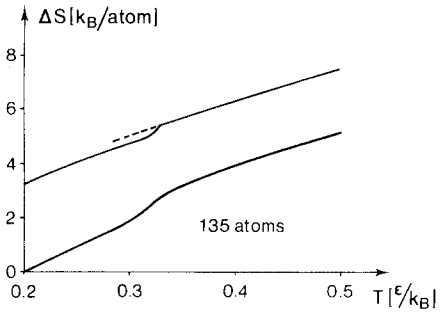

FIG. 6. Entropy variation with temperature for the 135-atom system. The upper curve is derived from vibrational spectra corresponding to the calculated points of the caloric equation of state. The uncertainty in entropy is ± 0.1. The lower curve is derived by integration of the specific heat curve. The accumulated error is estimated to reach a value of ± 0.4 at the highest temperature, whereas the accuracy of the entropy of fusion is about 0.04.

Contrary to what was found for the two-dimensional clusters treated in Ref. 9, no evaporation was observed in the three-dimensional systems for the temperatures considered here.

In Figs. 5–7 the entropy calculated from Eq. (9) is shown and compared with the results from the vibrational analysis [Eq. (11)]. The integration of c_P/T was carried out starting from $T = 0.2$. The upper curve of Fig. 6 shows that the vibrational analysis was able to detect a small shift in entropy for the 135-atom cluster upon melting. However, the fluctuations in the melting range are large and lead to statistical uncertainties in this range of the same order of magnitude as the shift itself.

The variation of the average distance between nearest-neighbor atoms with temperature is shown for the three systems in Fig. 8. This function is apparently also sensitive to structural changes within the cluster and the result with respect to the positions of the melt-

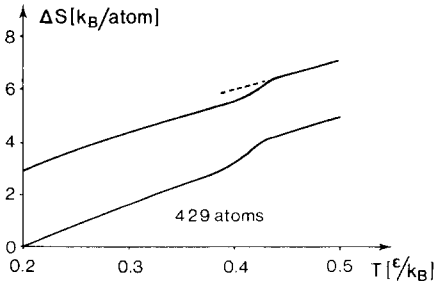

FIG. 7. Entropy variation with temperature for the 429-atom system. The upper curve is derived from vibrational spectra corresponding to the calculated points of the caloric equation of state. The uncertainty in entropy is ± 0.1. The lower curve is derived by integration of the specific heat curve. The accumulated error is estimated to reach a value of ± 0.4 at the highest temperature, whereas the accuracy of the entropy of fusion is about 0.05.

ing transitions of the three different clusters is in close agreement with the result of Fig. 4. The vibrational and structural properties of the clusters, calculated for the points A, B, C, and D on the caloric equation of state plot, are shown in Figs. 9–14. The frequency spectra, obtained from Eq. (12) and used in the calculation of the entropy, are shown in Figs. 9–11 for the different clusters at different temperatures. In all three figures the sequence from bottom to top, corresponding to the sequence $ABCD$, is: solid at a relatively two temperature, solid at a high temperature, liquid at the same temperature as the high temperature solid, and finally liquid just above the melting transition. In order to compare the frequency spectra for the different sizes of system, the curves are all normalized to unit area, and the low-temperature solid curves all apply to the same temperature (0.15).

All frequency spectra were calculated by averaging over eight velocity autocorrelation functions, each of which covered 500 computational cycles. Because of these limitations in time interval, as well as in the number of functions used in the averaging procedure, statistical fluctuations cannot be avoided and consequently the fine structure of the derived frequency spectra should be regarded with caution. By comparing the frequency spectra for different 4000-cycle periods calculated for the same total energy, it was found that although the relative heights of the peaks varied, the general shape was fairly constant. Figs. 12–14 show the pair distribution functions obtained as an average over 200 consecutive configurations with the central atom as datum point. The four curves correspond to the points A, B, C, and D going from bottom to top. These functions are also affected by statistical uncertainty. The fine structure that is revealed must to a great extent be attributed to this condition. The zero temperature properties and melting point parameters for the different clusters are listed in Table II and compared with the results for the infinite system. For the relaxed crystals at zero temperature the average nearest-neighbor distance UN_0, the binding energy $-\varphi_0$, and the distance from the central atom to the outermost atomic shell are given. The melting temperature, latent heat of fusion, and the entropy change upon melting, all derived from the caloric equation of state, are shown and compared with the entropy change obtained from the vibrational analysis.

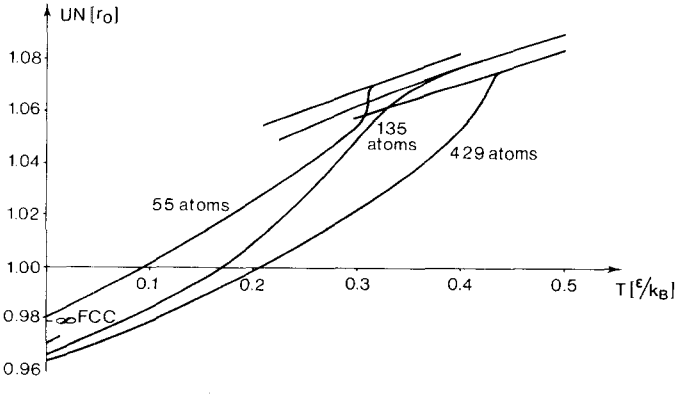

FIG. 8. Average nearest-neighbor distance as a function of temperature for the different cluster sizes. The low temperature metastable 55-atom fcc system is also shown.

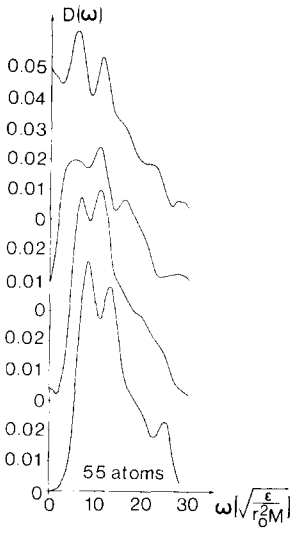

FIG. 9. Frequency spectrum of the 55-atom cluster. The distributions are calculated at the temperatures 0.148, 0.217, 0.211, and 0.341 going from bottom to top, corresponding, respectively, to the states labelled A, B, C, and D in Fig. 1. The distribution functions are normalized to unit area.

IV. DISCUSSION

The significance of the free surface to the structural and thermodynamical behavior of a microcrystal can be clearly seen from the caloric equation of state. Departures from equipartition, which must be attributed to the anharmonic part of the interatomic potential, appear even at low temperatures because of the surface atoms' weaker binding and consequently greater excursions from their equilibrium positions. The ratio of surface to bulk atoms must be decisive for the magnitude of this effect which shows up as a sort of premelting in the c_P curves. Apart from the 55-atom system, which in the solid phase adopts an icosahedral structure, and which thereby departs from the normal fcc behavior, this effect is greatest for the smallest system, as can be seen in Fig. 4. The depression of the melting point with respect to the bulk value, which is also due to the free surface, is also seen to be greatest for the smallest system. In must be emphasized that the c_P curves have been calculated on the basis of a heating situation, so they refer to the limit of stability for the structure rather than to an ensemble average for the system. During the calculation it was noticed that the system, which was originally in the solid phase, was able to jump over to the cooling curve after it had been in the transition region for some time. A similar phenomenon, which suggests that coexistence of the two phases is impossible in such small systems, has earlier been seen in computer experiments on systems with periodic boundary conditions.[21]

The time required for a jump to occur was found to be shorter the larger the energy of the system, corresponding to a larger transition probability as the limit of stability was approached. The lowest portion of the cooling curve was determined by cooling a liquid configuration and finding the equilibrium properties for different degrees of cooling in the same manner as for the case of heating. For the 55-atom system it was found, however, that the entire cooling curve shown could be

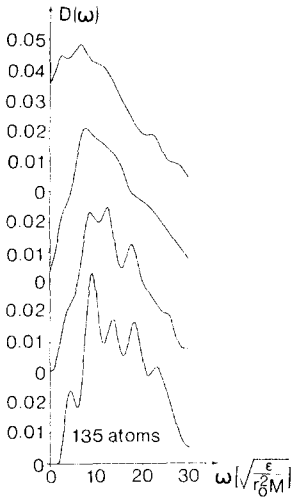

FIG. 10. Frequency spectrum of the 135-atom cluster. The temperatures are 0.152, 0.220, 0.222, and 0.387 from the bottom to top, corresponding to *A*, *B*, *C*, and *D*, respectively, of Fig. 2.

determined by a heating sequence (as described in Sec. II) starting out from the fcc structure. For values of the total energy lying between 0.15 and 0.75 the heated fcc microcrystal transformed after a few thousand time steps to an icosahedral packing. For energies larger than 0.75 the microcluster displayed equilibrium properties corresponding to the cooling curve.

The uncertainty in temperature for the heating curve in the transition region is ± 0.015, whereas for the other parts of the caloric equation of state it is ± 0.002 or less. Generally speaking, it can be said of the transition region that the uncertainty here is greatest because of the large temperature fluctuations. Furthermore, it was not possible to determine the ensemble average for these temperatures because the computational time was inadequate for determining the relative division between the solid and the liquid state. Figure 4, which was derived by graphic differentiation of the caloric equation of state curve, consequently has a significant uncertainty in peak height, while the melting temperature, which is given by the projection of the peak on the *T* axis is again characterized by an uncertainty of ± 0.015. Also for the unit curve in Fig. 8 the uncertainty in temperature is, in the transition region, ± 0.015, while in the remaining region it is ± 0.002.

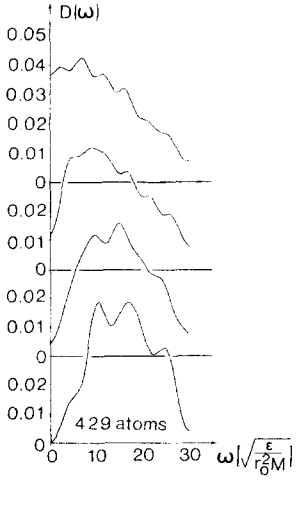

FIG. 11. Frequency spectrum of the 429-atom cluster. The temperatures are 0.153, 0.306, 0.309, and 0.442 from bottom to top, corresponding to *A*, *B*, *C*, and *D*, respecitvely, of Fig. 3.

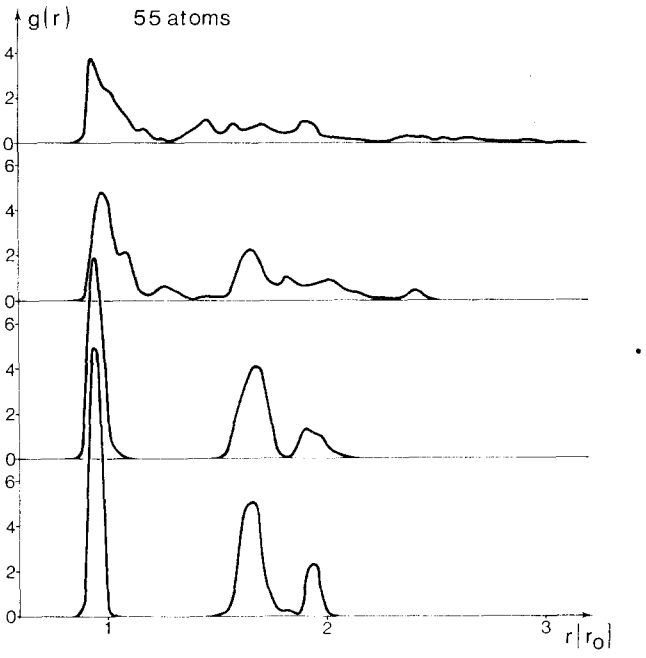

FIG. 12. Pair distribution functions of the 55-atom cluster calculated with the central atom is datum point. The sequence from bottom to top corresponds to the sequence *A*, *B*, *C*, and *D* of Fig. 1.

The history of the 55-particle system has recently been reviewed in a paper by Hoare and Pal.[6] It has now been rigorously shown that the icosahedral packing is more stable than all other isometric packings that have been considered as far as the potential energy is concerned. This has been shown for Lennard-Jones and Morse pair interactions. When considering only nearest-neighbor interactions the fcc or hcp "spherical" clusters, however, seem to be the ones with lowest potential energy. In the present calculations the Lennard-Jones potential was truncated midway between the fourth and fifth neighbors in the fcc system, and with this potential the icosahedral packing is obviously the most stable one. At low temperatures (less than $\simeq 0.015$) the spherical fcc cluster, however, seemed to be stable also in so far as it did not transform within a period of 20.000 time steps corresponding roughly to 150 atomic vibrational periods. Furthermore, the force constant matrix at zero temperature for the relaxed fcc structure was found to be positive definite.

For the two larger systems no structural transition in the solid phase could be observed, as seen in Figs. 2 and 3. This must be due to one of the following reasons, bearing in mind that the molecular dynamics method in principle explores all accessible regions of phase space:

(i) The fcc packing is the most stable one, in which case no transition will occur.

(ii) If any isomeric stable packing with lower free energy exists, no transition will occur if the barrier in free energy, which separates the two stable forms, is much larger than the kinetic energy of the system.

(iii) If the barrier in free energy is comparable to the

kinetic energy, a transition will occur. In this case, however, the difference in potential energy between the two isomeric packings must be negligible, i.e., within the uncertainty in temperature for the caloric equations of state.

In Figs. 13 and 14, which show the pair distribution function for the two larger systems, the arrows show the positions of the neighbor shells in the fcc structure, together with the corresponding number of atoms in these shells. It can be seen that the peaks corresponding to these neighbor shells can be recognized in the high-temperature solid state. This eliminates option (iii) of the possibilities listed above. It should be stressed that option (ii) cannot be eliminated on the basis of the calculations reported on here. Possible isomeric packings with lower free energy might exist, separated from the fcc packing by an energy barrier sufficiently high to prevent a transition even at temperatures close to the melting temperature. This problem can only be solved by a mutual comparison of all possible isomeric clusters.

When one compares the thermodynamic behavior of the microcrystals as a function of size, it transpires that in addition to the differences that have been described, there are pronounced tendencies with respect to relaxation, premelting, and latent heat. From Fig. 8 it is found that the average value of the nearest-neighbor distance, at zero temperature, increases from 0.9630 for the 429-atom system through 0.9658 for the 135-atom system to respectively 0.9700 and 0.9808 for

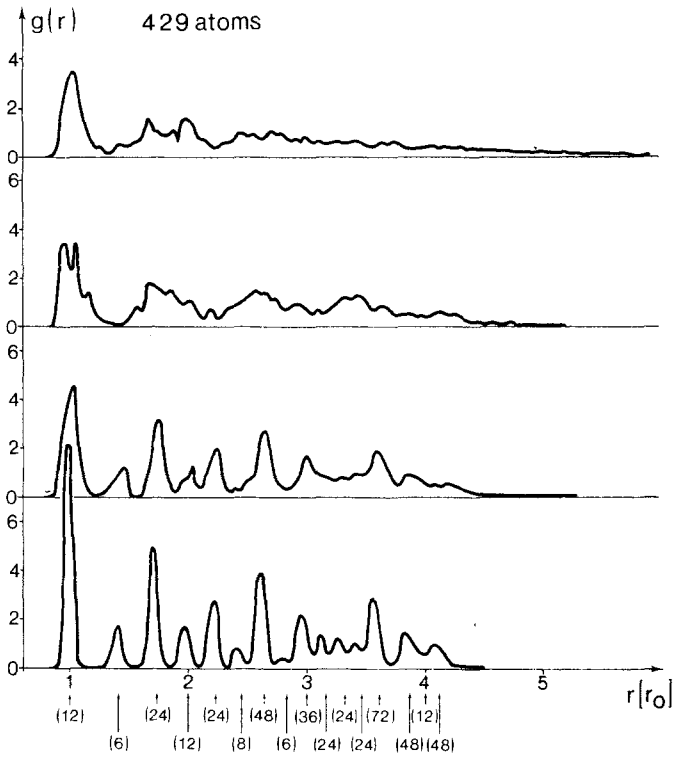

FIG. 14. Pair distribution functions of the 429-atom cluster calculated with the central atom as datum point. The sequence from bottom to top corresponds to the sequence *A*, *B*, *C*, and *D* of Fig. 3. The arrows on the abcissa give the positions of the neighbor shells in the fcc system. The corresponding figures give the number of neighbors contained in each shell.

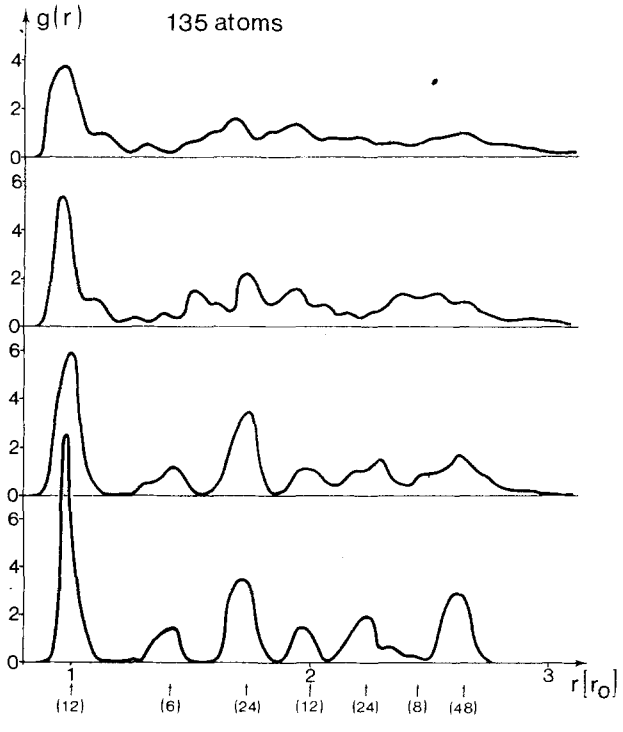

FIG. 13. Pair distribution functions of the 135-atom cluster calculated with the central atom as datum point. The sequence from bottom to top corresponds to the sequence *A*, *B*, *C*, and *D* of Fig. 2. The arrows on the abcissa give the positions of the neighbor shells in the fcc system. The corresponding figures give the number of neighbors contained in each shell.

the fcc and icosahedral variants of the 55-atom system. For an infinite system at zero pressure the corresponding value is 0.9784 for the same truncation of the potential.

Two effects are of special significance in connection with the mean nearest-neighbor distance in the relaxed microcrystal. The surface tension attempts to compress the system thereby lowering the mean distance. In the continuum approximation this effect should increase with decreasing crystal radius. From the atomistic point of view, however, the surface consists of a layer whose thickness is as large as the range of the potential, and for microcrystals that are so small that the surface accounts for a significant fraction of the crystal's volume another effect will be noticeable. The mean nearest-neighbor distance will be mainly determined by the relative positions of the surface atoms. The distance between these atoms will be greater than for the atoms at the core and in the limit as $N \to 4$ it will approach unity. The zero temperature relaxations show that this latter size effect is decisive for the crystal sizes studied here. Table II shows that for the fcc microcrystals the latent heat of fusion L_m is an increasing function of crystal size. The icosahedral structure is special in every respect since the mean nearest-neighbor distance is in this case larger than for the corresponding fcc structure, the latent heat of melting is much greater than one should expect from the tendency noted earlier in connection with the fcc structure, and the degree of premelting is less for the icosahedral

structure, as can be seen in Fig. 4. The special character of the icosahedral structure can be explained by the fact that this structure is simply more stable than the corresponding fcc structure.

The apparently conflicting results of on the one hand Briant and Burton[10] and the present authors and on the other hand McGinty[11] with respect to the existence of a fairly sharp transition from the solid to the liquid state might thus be explained in terms of the structure of the solid phase. The six different cluster sizes considered by McGinty, ranging from 15 to 100 atoms, are all characterized by low symmetry in the solid phase. In fact none of the clusters can be obtained as spherical clusters of some specified packing type. In this case the decrease in latent heat of melting and increase in premelting with decreasing cluster size is strong enough to obscure the transition effectively. The 55-atom cluster considered by Briant and Burton and included also in the present work, in contrast, attains a closed spherical form of icosahedral packing sufficiently stable to override the above-mentioned trends.

Previous calculations of the vibrational entropy of 55-atom argon clusters[6,20] reveal a significant departure from the results obtained in the present study. These calculations are based on the harmonic approximation and are applied at temperatures up to about 80 °K. The melting point for the classical system treated here, fitted to argon, was found to be 36.6 °K, and the agreement between the two calculations is consequently rather poor. The thermodynamic calculation of entropy, using Eq. (9), is in principle exact for the classical system and the results obtained by it will be used as a basis for evaluating the method of Dickey and Paskin.[16] Esbjørn *et al.*[17] showed that results obtained by the latter are about 8% lower than those obtained by the thermodynamic approach, when applied to an infinite system. For the microcrystals the discrepancy is about 19% in the same direction, neglecting the jump at the transition which shows a discrepancy of about 27%. From expression (11) for the entropy one sees that it is the lowest frequencies that make the largest contribution to the entropy, and that it is just these frequencies that are imbued with the greatest uncertainty because of the limited time used to determine the velocity autocorrelation function. One should expect the entropy calculation to be worse under those conditions in which the low frequency part of the spectrum is changing most abruptly, i.e., during the phase change when the diffusive modes begin to appear to an appreciable extent. The poor over-all agreement between the thermodynamic and frequency-analysis results in the calculations reported here can be attributed to the presence of the free surface in that this creates the possibility for surface diffusion and is characterized by a looser binding of the atoms compared to the situation in the bulk material. This effect shows up in the frequency spectra of Figs. 9–11, and it is already visible in the solid phase because $D(\omega = 0) \neq 0$ in the high-temperature curves for all three crystal sizes.

From the pair distribution curves corresponding to the frequency spectra of Figs. 12–14, it appears that the high-temperature solid has a diffuse surface and that the low-frequency modes reported here are due mainly to the free surface. For the liquid state at the same temperature as the high-temperature solid it can be seen from the pair distribution that there is just as diffuse a surface layer as for the solid. The frequency spectra show however that low-frequency modes are present to a much greater extent than in the solid, which must be due to the considerable self-diffusion that occurs in the liquid phase. Briant and Burton calculated the radial and angular contributions to the self-diffusion coefficient arising from the individual atomic shells of the 55-atom icosahedron. Their results are in close agreement with the picture of diffusion that emerges from the results presented here. The pair distribution functions also show the pronounced liquid character of the inner part of the crystals. The next-nearest-neighbor peak of the fcc structure is replaced by a minimum, which is a well-known characteristic of the liquid phase.[14] The high-temperature liquid's pair distribution functions show that the surface in this case is still more diffuse so that surface diffusion can be expected to be even more pronounced and this will contribute strongly to the marked increase in $D(\omega = 0)$ from the low- to the high-temperature liquid situations.

TABLE II. Zero temperature properties and melting parameters for the microcrystals compared with the result for the infinite system. The melting parameters of the infinite fcc system are average values of the experimental data[19] for Ar, Kr, and Xe, presented in reduced units.

	UN_0	$-\varphi_0$	R_{syst}	T_M	L_M	S_M^{ces}	S_M^{vib}
55 Ico.	0.980751	4.9918	1.908	0.310	0.357	1.15	0.80
55 fcc	0.969982	4.7653	1.971	...	...	...	...
135 fcc	0.965848	5.5432	2.598	0.325	0.130	0.40	0.30
429 fcc	0.963032	6.2431	4.035	0.420	0.273	0.65	0.48
∞ fcc	0.978416	7.8803	...	0.685	1.168	1.71	...

The broad features of the frequency distribution in the low-temperature solids are in agreement with those observed by Dickey and Paskin[8] for small particles. Remnants of the longitudinal bulk modes that appear in the high-frequency end of the spectrum are seen to have less importance the smaller the crystals are, whereas the peak located at about $\omega = 9$ becomes more dominant. Dickey and Paskin identified this peak as a surface mode with amplitude normal to the surface while the shoulder located at about $\omega = 5$ was linked to edge atoms. This edge mode is seen to grow with decreasing crystal size, because of the larger surface to volume ratio, while for the 55-atom system it disappears completely, apparently because of the icosahedral structure's surface composition. The over-all features of the 429-atom system are in accord with Dickey and Paskin's results for their spherical droplet and their five layer particle while the 135-atom system shows properties corresponding to their three-layer particle consistent with the above-mentioned significance of the surface to bulk ratio for the crystal's frequency spectrum.

The definition of a physical cluster adopted in the present work, i.e., the boundary condition that was applied, is, for the cluster sizes considered, very similar to that of Lee *et al.*[12] and of McGinty.[11] It should be noted, however, that for larger clusters a boundary

condition based on a constant ratio of constraining volume to bulk volume occupied by the number of atoms in the cluster would ultimately yield situations where the cluster is able to split up into smaller, noninteracting clusters within the constraining volume. Such situations would not be possible with the boundary condition used in the present studies, which gives the constraining volume as the bulk volume of the cluster plus a "surface" volume of a thickness comparable to the effective range of the interatomic potential.

V. CONCLUSION

With the molecular dynamics method it has proved possible to simulate the behavior of small clusters of atoms over a temperature range which includes the melting transition. The observed melting points show that the results calculated on the basis of the harmonic approximation frequently extrapolate to temperatures well above the melting point. It therefore appears to be clear that the theoretical treatment of microcluster properties at elevated temperatures should be based on dynamic methods.

The most noteworthy results of the calculations reported here are that the microcrystals melt by suddenly switching to the liquid phase, a condition which suggests that coexistence between the two phases is not possible in these systems. The crystals melt, therefore, not by gradually changing configuration from the surface in towards the center, but by an abrupt rearrangement of the bulklike core, which during the process continues to be surrounded by a diffuse surface of a certain (constant) thickness.

[1]J. G. Allpress and J. V. Sanders, Aust. J. Phys. **23**, 23 (1970).
[2]J. J. Burton, J. Chem. Phys. **52**, 345 (1970).
[3]J. J. Burton, Chem. Phys. Lett. **7**, 567 (1970).
[4]F. F. Abraham and J. V. Dave, J. Chem. Phys. **55**, 1587 (1971).
[5]F. F. Abraham and J. V. Dave, J. Chem. Phys. **55**, 4817 (1971).
[6]M. R. Hoare and P. Pal, J. Cryst. Growth **17**, 77 (1972).
[7]D. J. McGinty, Chem. Phys. Lett. 13, 525 (1972).
[8]J. M. Dickey and A. Paskin, Phys. Rev. B **1**, 851 (1970).
[9]R. M. J. Cotterill, W. D. Kristensen, J. W. Martin, L. B. Pedersen, and E. J. Jensen, Comput. Phys. Commun. **5**, 28 (1973).
[10]C. L. Briant and J. J. Burton, Nat. Phys. Sci. **243**, 100 (1973).
[11]D. J. McGinty, J. Chem. Phys. **58**, 4733 (1973).
[12]J. K. Lee, J. A. Barker, and F. F. Abraham, J. Chem. Phys. **58**, 3166 (1973).
[13]B. J. Alder and T. Wainwright, J. Chem. Phys. **31**, 459 (1959).
[14]A. Rahman Phys. Rev. **136**, A405 (1964).
[15]L. Verlet, Phys. Rev. **159**, 98 (1967).
[16]J. M. Dickey and A. Paskin, Phys. Rev. **188**, 1407 (1969).
[17]P. O. Esbjørn, E. J. Jensen, W. D. Kristensen, J. W. Martin, and L. B. Pedersen, J. Comp. Phys. **12**, 289 (1973).
[18]P. A. Egelstaff, *An Introduction to the Liquid State* (Academic, New York, 1967), Chap. 2.
[19]G. L. Pollack, Rev. Mod. Phys. **36**, 748 (1964).
[20]D. J. McGinty, J. Chem. Phys. **55**, 580 (1971).
[21]B. J. Alder and T. E. Wainwright, Phys. Rev. **127**, 359 (1962).